Clay Minerals (1998) **33**, 231–241

Ga/Al substitutions in synthetic kaolinites and smectites

F. MARTIN, S. PETIT*, A. DECARREAU*, PH. ILDEFONSE**, O. GRAUBY†, D. BEZIAT, PH. DE PARSEVAL AND Y. NOACK‡

*Université Paul Sabatier, Laboratoire de Minéralogie-Cristallographie, UMR 5563 CNRS, 39 Allées Jules Guesde, F-31000 Toulouse, *Université de Poitiers, Laboratoire 'Hydr.A.S.A.', URA 721 du CNRS, 40 Avenue du Recteur Pineau, F-86022 Poitiers Cedex, **Universités Paris 6 et 7, Laboratoire de Minéralogie-Cristallographie, CNRS 09 et IPGP, 4 Place Jussieu, F-75252 Paris Cedex 05, †CRMC2-CNRS, Campus Luminy, Case 913, F-13288 Marseille Cedex 9, and ‡Université d'Aix-Marseille III, Laboratoire de Géosciences de l'Environnement, CNRS FU 017, Europôle Méditerranéen de l'Arbois, BP 80, F-13545 Aix en Provence Cedex 4, France*

(*Received 16 December 1996; revised 14 May 1997*)

ABSTRACT: The Ga for Al substitution in kaolinites and smectites was studied using clay synthesis from initial gels having an (Al + Ga)/Si ratio of kaolinites and *M*Ga = Ga/(Ga + Al) ratio ranging from 0 to 1. Only kaolinite was obtained for *M*Ga in the range 0−0.10. For higher *M*Ga, synthesized clays were both kaolinite and beidellite, or pure beidellites. The evolution of *b* cell parameters, and the appearance of a νAl-OH-Ga absorption band at 3600 cm^{-1} in FTIR spectra, proves the progressive substitution of Al by Ga in kaolinite. The low substitution of Al by Ga in kaolinite can be correlated with the large difference in ionic radii between Al^{3+} and Ga^{3+} which causes a large increase in cell dimensions. By contrast, the incorporation of Ga in smectites is easy and can be complete.

Large supplies of Ga have been needed since 1990 and this requirement will extend well into the 21st century. According to Katrak & Agarwal (1981) the most promising source is bauxite from which Ga is extracted.

Hiéronymus *et al.* (1990) showed that in classical ferralitic weathering of various rocks, Ga is mostly associated with Al in potassic feldspars, plagioclases, kaolinite and gibbsite. In bauxites, even though Ga is expected to substitute for Al in Al hydroxides, it may also occur in kaolinites.

The purpose of this work was to examine the possibility of Ga incorporation in synthetic Al clay minerals (kaolinite and smectite) and to obtain mineralogical data. Hydrothermal syntheses of clay minerals with various Ga contents were performed at 200°C.

EXPERIMENTAL TECHNIQUES

Initial material

Eleven gels were prepared following the procedure described by Petit & Decarreau (1990) using sodium metasilicate ($SiO_2Na_2O{\cdot}5H_2O$), and aluminium and gallium nitrates ($Al(NO_3)_3{\cdot}9H_2O$ and $Ga(NO_3)_3{\cdot}9.5H_2O$), according to the following precipitation reaction:

$$2SiO_2Na_2O + (2-x)Al(NO_3)_3 + xGa(NO_3)_3 + 2NaOH \rightarrow Si_2Al_{2-x}Ga_xO_7 + 6NaNO_3 + H_2O \quad (1)$$

Gels with different compositions were prepared, with x varying from 0 to 2. After precipitation, the solid phase was centrifuged and washed to remove sodium nitrate. Gels were then treated at 60°C for 12 h and finally crushed.

Hydrothermal ageing

A 210 mg quantity of powdered gel and 30 ml of distilled water were placed in Teflon-coated metal bombs which were held for 30 days at 200°C (±3°C) under water pressure equilibrium (almost 16 bars). The pH conditions were acidic (pH = 1−1.5). The final products were filtered, washed, dried and gently ground.

Analytical procedures

All products were examined by X-ray diffraction (XRD) in reflection mode using a Philips PW1730 diffractometer with Fe-filtered Cu-*K*α radiation (40 kV, 40 mA), combined with a DACO-MP computer. The *d*(001) of kaolinites was measured from oriented preparations.

The chemical analyses of bulk samples were performed using a CAMECA SX 50 microprobe (wavelength dispersive spectrometer (WDS) analysis) in the 'Laboratoire de Pétrographie', University of Paris VI. The analytical conditions were as follows: accelerating voltage of 15 kV, beam size of 1000 nm, beam current of 3.38 nA, counting time of 10 s for each analysed element.

Cation exchange capacity (CEC) was determined using the Jackson method (1958), with sodium acetate at pH = 7.

Transmission electron microscopy (TEM) observations were made with a JEOL 2000 FX microscope, using samples dispersed on a carbon-coated microgrid (C.R.M.C.2, Marseille, France). Spot analyses were obtained by analytical electron microscopy (AEM), using the same microscope (200 kV accelerating voltage) equipped with an energy dispersive X-ray spectrometer (EDX, Tracor Northern Si(Li) detector). In fixed transmission mode, the spot size diameter ranged from 400 to 1000 Å. The thickness of the particles analysed being <1000 Å, quantitative data were obtained by the thin-film method (Cliff & Lorimer, 1975) after calibration of the $k_{x,Si}$ factors (x = Al, Ga) using natural and synthetic layer-silicates of known and homogeneous compositions.

Fourier transform infrared (FTIR) spectra were recorded in transmission mode in the 4000−400 cm^{-1} range on a Nicolet 510 FTIR spectrometer. The pellets were prepared by mixing 4 mg sample with 300 mg KBr.

The XANES experiments were run at the French synchrotron facility (LURE, Orsay), on the D44 station. The DCI storage ring was operated at 1.85 GeV and 200 mA. A Si (311) double crystal was used to monochromatize the X-ray beam. The XANES spectra at the Zr *K*-edge were collected in transmission mode at room temperature with energy steps of 0.5 eV over the 10350−10430 eV energy range. Spectra were calibrated by reference to metallic Ga (Ga *K*-edge at 10367 eV). The two samples (3 and 10) and the references with various Ga coordination number 4 or 6 (αGaOOH, nepheline structure ($GaGe_2O_6Na$) and $AsGaO_4$) were finely ground and the resulting powders were sandwiched between two pieces of kapton tape. Sample absorbance was controlled by adjusting the sample thickness.

RESULTS

Chemical analyses

Measured *M*Ga (*M*Ga = Ga/Ga+Al) of the synthesized products are roughly the same as the calculated one after the precipitation reaction (1) (Table 1), revealing a non-selective incorporation of these elements in the solid phase.

From samples 1 to 4, the SiO_2 contents of synthesized products are equal to, or a little lower than, calculated according to the quantities used for the syntheses. However, for samples 6 to 10, this trend is reversed with higher SiO_2 contents than expected. On a ternary diagram (Fig. 1), the chemical compositions of bulk samples, measured by WDS and AEM analyses are located within an area defined by both chemical compositions calculated for Al-kaolinite–Ga-kaolinite and Al-beidellite–Ga-beidellite (Fig. 1), except for some samples (2-3-4) which have lower SiO_2 contents than expected. As the Ga content increases (samples 8 to 10), the chemical data plot clear of the kaolinite line and become closer to the beidellite one.

The AEM analyses of individual particles of the samples 4 and 6 are also reported on Fig. 1. For these samples, particles show higher amounts of SiO_2 than the bulk material. For sample 4, although the bulk chemical analysis is outside the Al-Ga-kaolinite-beidellite domain, the AEM chemical compositions measured by TEM on particles fall inside, and show variations in *M*Ga close to the Ga-Al-kaolinite line. For sample 6, the chemical compositions of particles are clearly in the smectite domain.

TABLE 1. Description of the synthesized samples.

Samples	Calculated chemical composition (%)*			Expected *M*Ga*†	Measured *M*Ga†	XRD characterization
	SiO_2	Al_2O_3	Ga_2O_3			
1	54.0	46.0	0.0	0.00	0.00	K
2	53.0	42.8	4.2	0.05	0.05	K
3	52.0	39.8	8.2	0.10	0.10	K
4	49.3	31.4	19.3	0.25	0.24	K, S
5	47.6	26.3	26.1	0.35	#	K, Ox
6	46.2	21.5	32.3	0.45	0.28	K- S (95/5)‡
6b	46.2	21.5	32.3	0.45	#	S
7	45.3	19.1	35.6	0.50	#	K-S (90/10)‡, K
8	44.0	15.0	41.0	0.66	0.49	K-S (90/10)‡, S
9	40.1	3.4	56.5	0.90	0.81	S
10	39.0	0.0	61.0	1.00	1.00	S

* according to reaction (1)
\# not available
† *M*Ga = Ga/(Ga + Al)
‡ % of interstratified minerals, estimated after NEWMOD calculations (Reynolds, 1985)
K: kaolinite; S: smectite; K-S: interstratified kaolinite-smectite; Ox: oxides

From samples 1 to 3, the CEC of the synthesized products are very low, from ~0 to 4 mEq/100 g (Fig. 2), and are in accordance with CEC values measured for kaolinites. From samples 4 to 8, the CEC increases with the Ga content. For samples 9 and 10, the CEC of ~125 mEq/100 g is common for smectites (Środoń *et al*., 1986). The CEC values of samples with intermediate *M*Ga can be explained by a physical mixture and/or mixed-layer of kaolinite and smectite-like clays.

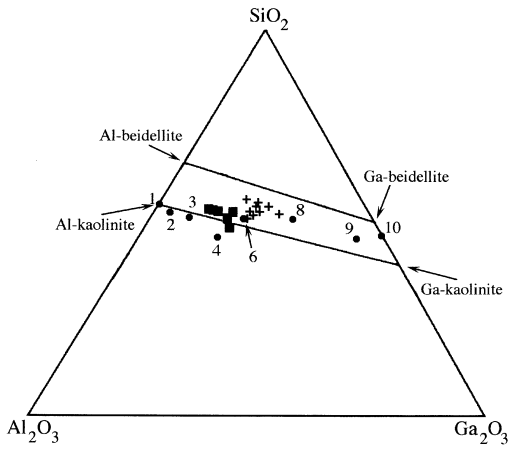

FIG. 1. Results of WDS (l) and AEM chemical analyses (■: sample 4; +: sample 6) plotted on a SiO_2–Al_2O_3–Ga_2O_3 ternary diagram. The Al-beidellite $[Na_{0.33}Al_2(Si_{3.67}Al_{0.33})O_{10}(OH)_2]$ is from Nesbitt (1977) and the Ga-beidellite is the corresponding calculated Ga end-member $[Na_{0.33}Ga_2(Si_{3.67}Ga_{0.33})O_{10}(OH)_2]$.

X-ray diffraction

The XRD powder patterns of synthesized products vary significantly with their Ga contents

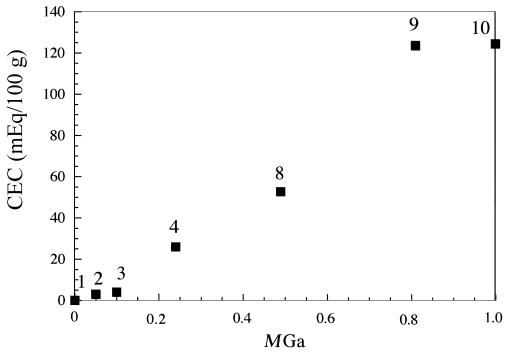

FIG. 2. The CEC *vs*. *M*Ga diagram of the synthesized products described in Table 1.

(Fig. 3). Some sharp reflections corresponding to Na salts (due to incomplete washing of samples after synthesis) are sometimes observed (see sample 8).

From samples 1 to 3, the XRD powder patterns are clearly those of kaolinite. From sample 4 to 6, kaolinite is the main component. A broad shoulder near 12 Å, which shifts slightly after glycolation (Fig. 4), reveals the occurrence of smectite.

The XRD pattern of samples 7 and 8 are similar and prove the presence of kaolinite-smectite (K-S) interstratified clay minerals (Table 1).

The XRD patterns of samples 9 and 10 are characteristic of smectites. The basal reflections are near 12 Å, characterizing a Na-smectite with one water layer. All the layers expand to about 16.9 Å when glycolated (Fig. 4). The Li test (Hoffmann & Klemen, 1950; Greene-Kelly, 1953) was used to determine the origin of the negative layer-charge of these smectites. After Li^+ saturation, heat treatment and contact with ethylene glycol, all the smectite layers expand and an intense peak at 17.5 Å can be observed. This is typical of smectite having a partly tetrahedral charge (i.e. beidellite).

Cell dimensions are related to the ionic radius of the constituent atoms and frequent use is made of the 060,331 spacing in predicting octahedral composition. Precise measurements (with LiF internal XRD standard) of the *d*(060,331) value were made and it was shown that it increased with *M*Ga (Fig. 5). For the highest *M*Ga, the 060,331 reflection appears at a high value for a dioctahedral smectite (1.51 Å) but is consistent with an octahedral sheet completely filled by Ga^{3+} cations.

Transmission electron microscopy observations

The TEM observations of synthetic clays (made on samples 4 and 6) establish two main particle morphologies (Fig. 6a,b). Sample 4 contains well-developed pseudo-hexagonal plates which is a morphology usually observed for kaolinites (Plançon & Tchoubar, 1977; Tomura *et al*., 1985). The electron

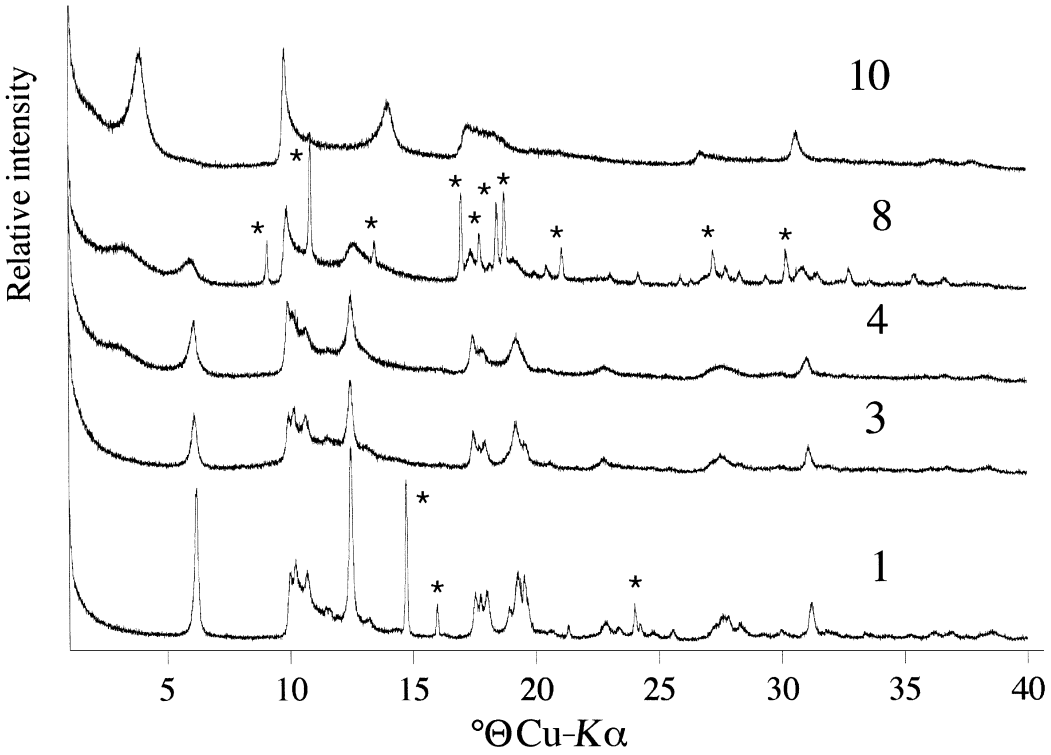

FIG. 3. XRD powder patterns of the synthesized samples described in Table 1. *: residual salt.

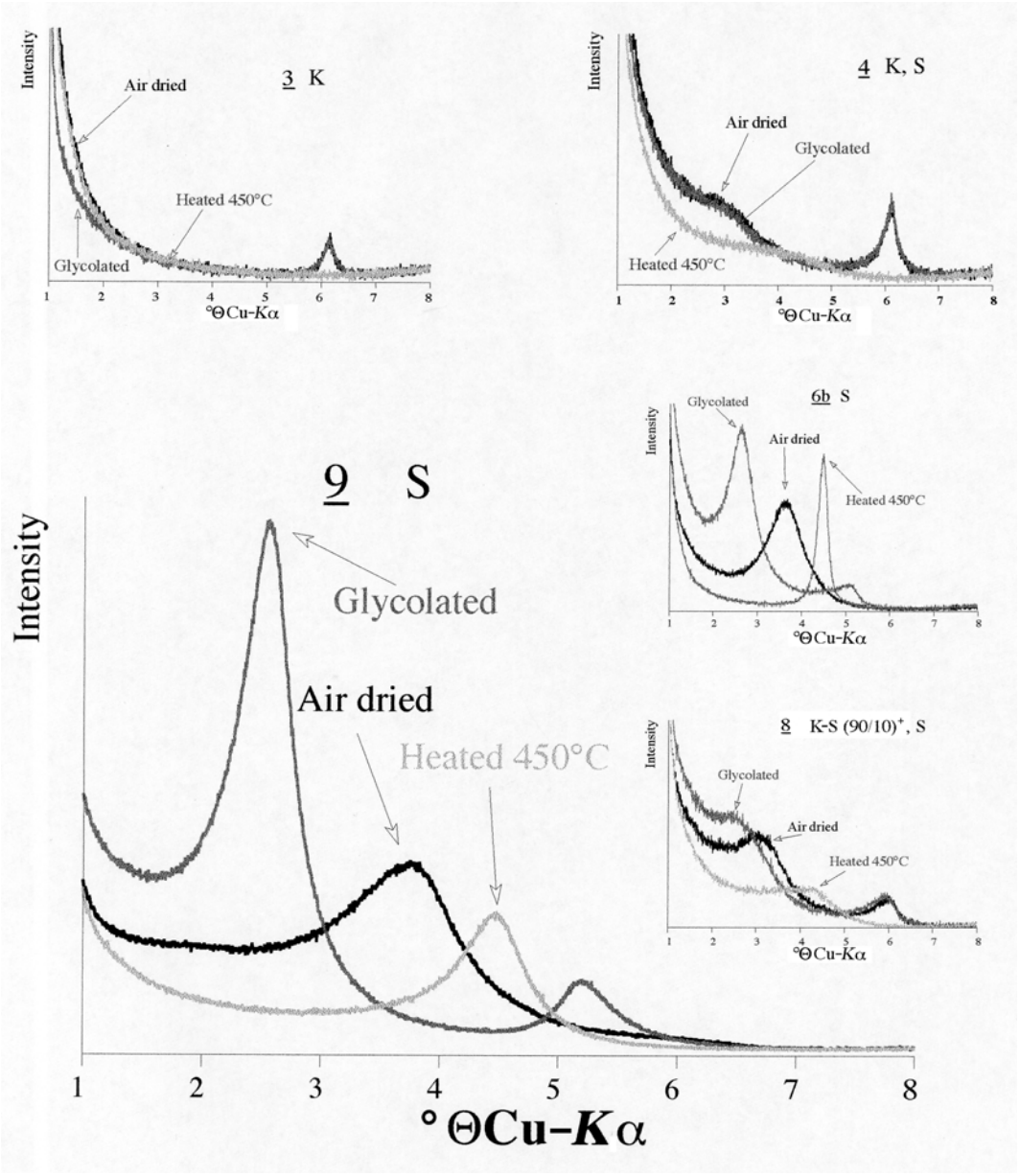

FIG. 4. XRD patterns (air dried, glycolated, and heated) of various oriented samples.

diffraction patterns (Fig. 6c) are composed of spots forming an hexagonal network corresponding to *hk* reflections. The *d*(060,331) value which can be measured is close to 1.49 Å (±0.01 Å).

In sample 6, two particle morphologies are observed: irregular folded and crumpled sheets are mixed with pseudo hexagonal plates (Fig. 6b). Electron diffraction patterns contain contributions from hexagonal networks of spots and rings, corresponding to similar *hk* spacings. This sample appears clearly as a mixture of kaolinite and smectite particles.

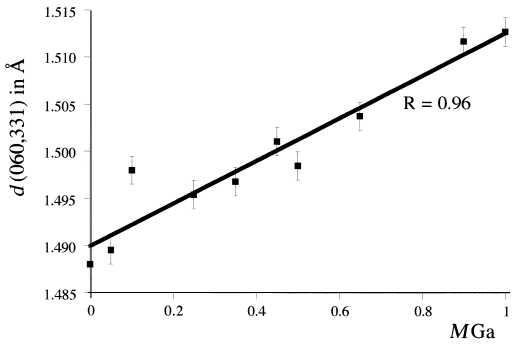

FIG. 5. d(060,331) measured on XRD patterns *vs*. *M*Ga of the synthesized products.

Infrared spectroscopy

The OH-stretching region. The FTIR spectra change notably along the series of samples (Fig. 7). The IR spectrum of sample 1 is typical of Al-kaolinite (Barrios *et al*., 1977; Rouxhet *et al*., 1977; Lietard, 1977; Cases *et al*., 1982) with four νOH absorption bands located at 3691, 3667, 3650 and 3620 cm^{-1}, and attributed to νAl_2OH.

The small band at 3434 cm^{-1} is commonly observed on the IR spectra of synthetic kaolinites (De Kimpe *et al*., 1981; Tomura *et al*., 1985; Petit & Decarreau, 1990) as well as natural samples (Kato *et al*., 1977; Delineau *et al*, 1994) but has not been assigned.

Up to sample 8, as the Ga content increases, kaolinite features can be observed on the IR spectra but became more and more altered.

From sample 2, an additional absorption band located at 3599 cm^{-1} appears. This band is close to the one due to νAl-OH-Fe vibrations (3598 cm^{-1}) in kaolinites (Petit & Decarreau, 1990) or smectites (Petit *et al*., 1995). It can be unambiguously attributed here to νGa-OH-Al vibrations because the samples are depleted in Fe. The proximity of these two bands can be explained by the similar atomic weight and by the similarity in ionic radii of Fe^{3+} and Ga^{3+} cations in octahedral sites. These νGa-OH-Al absorption bands increase in intensity along the series, reflecting the increase in of Ga/Al substitutions in octahedral sheets of smectites and possibly kaolinite.

From sample 4 (not shown) to 8, the spectra show broad features which can be interpreted by a superposition of IR spectra of kaolinites more or less substituted by Ga, and Ga-rich smectites. Notably, a shoulder appears near 3579 cm^{-1} from sample 4, and increases progressively. It becomes a single intense band for samples 9 and 10 which are characteristic of Ga-smectites. This band which is attributed to νGa_2OH vibrations in smectites (Stubican & Roy, 1961) indicates Ga-Ga neighbour relationships as early as sample 4. Clear features due to νGa_2OH vibrations in kaolinite were not observed.

The 1200–400 cm^{-1} region. The main absorption band close to 1030 cm^{-1} (ν_{Si-O}) remains at the same location along the series for the clay skeleton (Fig. 8). The only difference is the progressive disappearance of the band located at 1114 cm^{-1} clearly distinguishable for kaolinite samples. This disappearance is followed by a broadening of the main absorption band with the *M*Ga increase.

In the 600–400 cm^{-1} region, similar observations are made: modulations are observed for kaolinite samples and disappear for smectitic ones. The $Si-O-Al^{VI}$ absorption band, located at 543 cm^{-1} in kaolinite (Farmer, 1974) is observed from samples 1 to 3. With the *M*Ga increase, a progressive shift of this band towards the low wavenumber side is observed (517 cm^{-1} for samples 9 and 10). This last absorption band corresponds to vibrations of $Si-O-Ga^{VI}$ in smectites (Stubican & Roy, 1961).

Considering the OH-bending region, δAl_2OH bands are observed at 914 and 940 cm^{-1} from samples 1 to 3, as commonly seen in kaolinites (Farmer, 1974). The 940 cm^{-1} shoulder, characteristic of kaolinite, disappears progressively up to sample 6. The 914 cm^{-1} band which can be due to δAl_2OH in kaolinites or smectites, shifts towards the lower wavenumber side (903 cm^{-1} for samples 9 and 10) with increasing *M*Ga. This band at 903 cm^{-1} is attributed to δGa_2OH in smectite by Stubican & Roy (1961). A slight shoulder near 853 cm^{-1} can be attributed tentatively to δAl-OH-Ga in smectites. Unlike the νOH region results, a clear δAl-OH-Ga band for kaolinite cannot be detected.

XANES

The Ga *K*-edge XANES spectra of the two investigated materials (samples 3 and 10) are shown in Fig. 9, along with reference samples with tetrahedrally coordinated or octahedrally coordinated Ga. The edge-crests are located at 10397.33 and 10401.01 eV ($\pm$0.1 eV) for IV and VI coordinations, respectively.

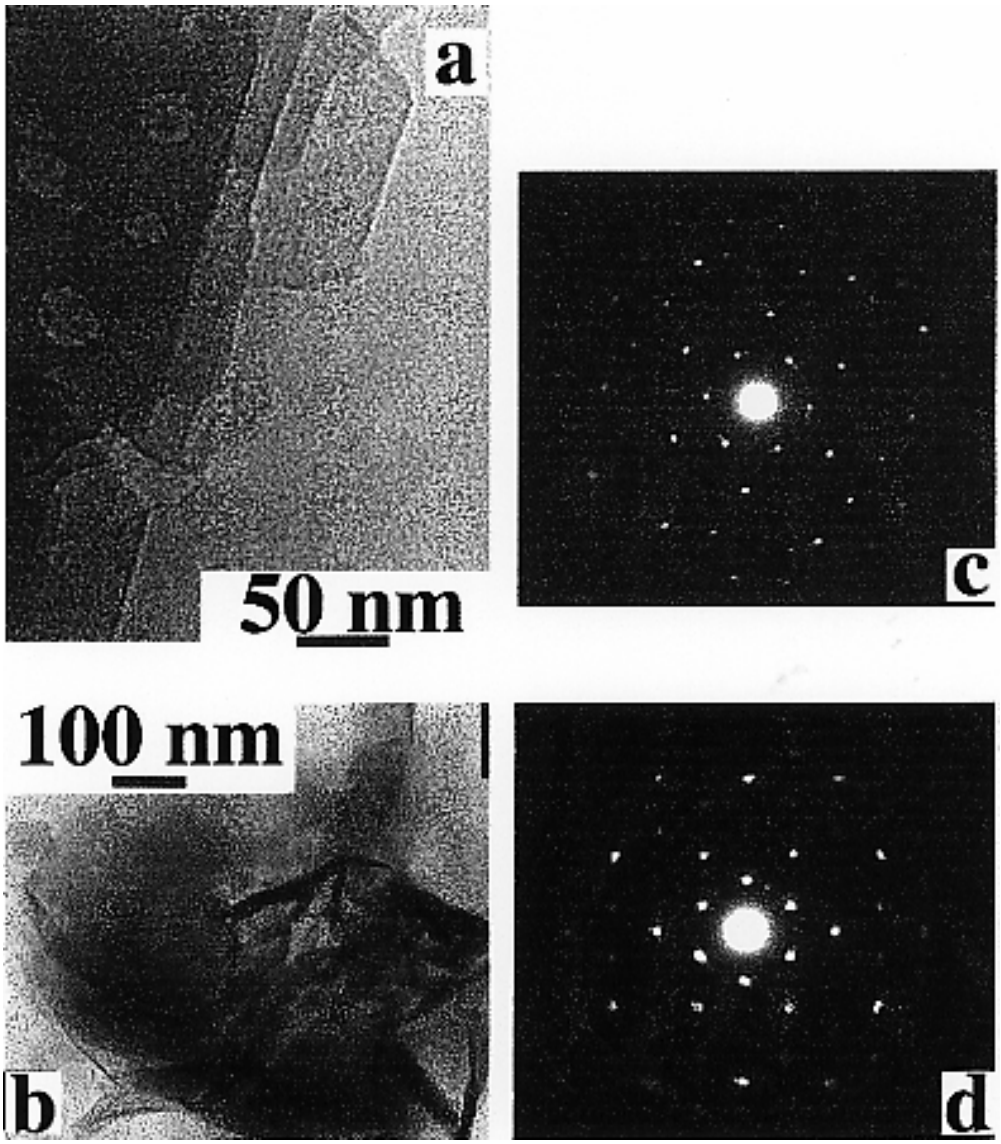

FIG. 6. TEM pictures and corresponding electron diffraction patterns of samples 4 [(a) and (c)] and 6 [(b) and (d)].

The spectrum of sample 3 shows the only 6 coordination number for Ga, in accordance with Ga in the octahedral sheet. The spectra of sample 10 give a broad band resulting from a mixture of the two Ga coordinations indicating a clear occurrence of tetrahedral Ga. This result confirms the tetrahedral charge of synthetic smectite due to Si/Ga^{3+} substitutions in its tetrahedral sheet.

DISCUSSION AND CONCLUSIONS

Previous syntheses of Ga-clays were concerned only with smectites with octahedra completely filled by Ga and obtained below 100°C (Siffert & Wey, 1961) or at 500°C (Stubican & Roy, 1961).

Despite the fact that the initial gels were prepared with the (Al + Ga)/Si ratio of kaolinite, only a few

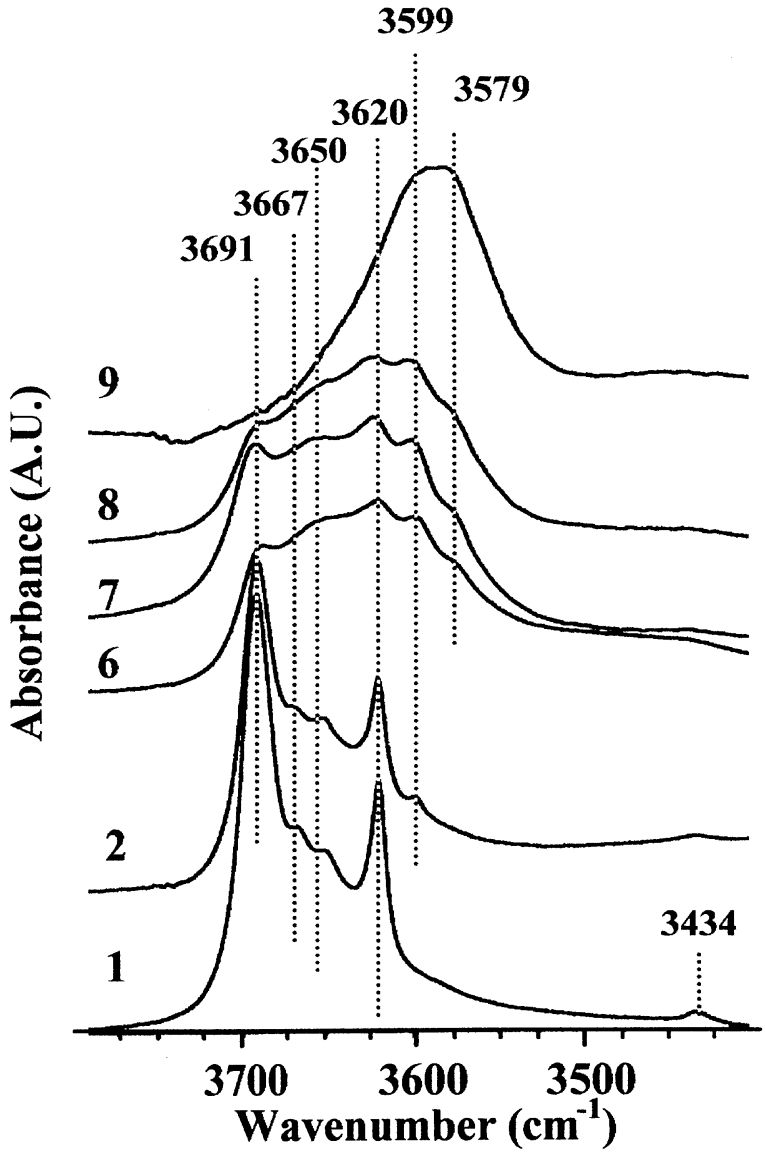

FIG. 7. FTIR spectra in the OH-stretching region of some synthesized samples described in Table 1.

synthetic clays appear as pure kaolinites. The XRD data and the microprobe and AEM chemical analyses corroborate these results.

For samples 1 to 3, which are pure kaolinite with Al having been partially substituted by Ga, a clear increase in *b* parameters can be observed. This evolution of this parameter is consistent with the larger size of Ga^{3+} (0.62 Å) in comparison with Al^{3+} (0.53 Å) (Shannon, 1976). The measured increase of the *b* parameter is large and, on the basis of these data, the expected *d*(060,331) of the fully substituted Ga-kaolinite would be near 1.54 Å. Such a value seems to be too high for a 1:1 silicate clay, and would explain why it is unlikely that a Ga-kaolinite could be synthesized, at least for our temperature synthesis. According to the present data, Ga can substitute for Al in kaolinite structures until the *M*Ga values reach

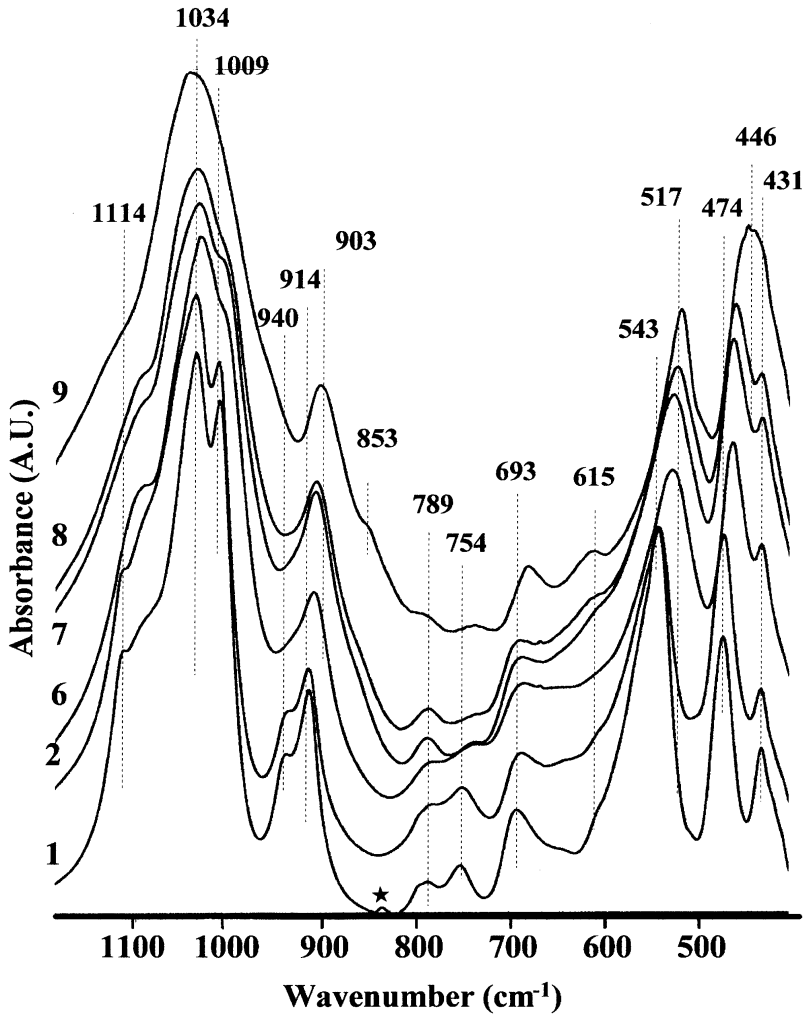

FIG. 8. FTIR spectra in the 1200−400 cm^{-1} region of some synthesized samples described in Table 1. *: residual salt.

0.10. Petit & Decarreau (1990) synthesized Fe^{3+}-substituted kaolinites, in similar conditions to those used here and obtained synthetic kaolinite with an Fe/(Fe + Al) ratio near 0.1. The substitution rates for Ga^{3+} and Fe^{3+} cations are similar probably because the sizes of their ionic radii are in the same range. Even if Al/Ga substitution levels in synthetic kaolinites seem to be limited, natural kaolinites would be able to contain much more Ga than a few ppm in their structure from a crystallochemical point of view.

For *M*Ga contents >0.1, Ga appears to precipitate in smectite. These results are consistent with the previous works of Siffert & Wey (1961) and Wolf (1967) who found that it was easier to synthesize Ga-smectite than Ga-kaolinite (kaolinite was not obtained). The CEC has been qualitatively used to estimate the number of smectitic layers in the synthetic clays. When the CEC is <10 mEq/100 g, the amount of smectite is very small. From these data, samples 4 to 8 are found to contain increasing amounts of smectite layers as shown by XRD and IR data. The CEC are those of smectites for samples 9 and 10.

Sample 10 is clearly a pure smectite; its structural formula calculated using chemical data

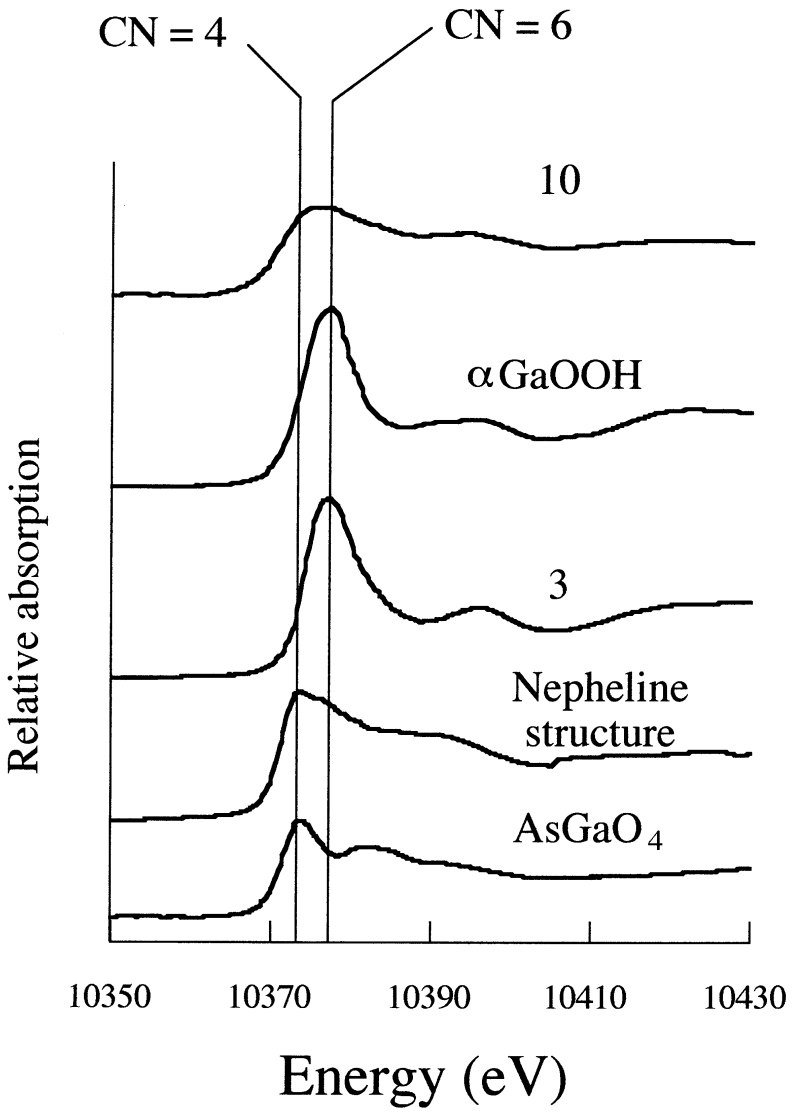

FIG. 9. XANES spectra of samples 3 and 10 described in Table 1 and of various minerals (αGaOOH, nepheline structure ($GaGe_2O_6Na$) and $AsGaO_4$) with octahedral or tetrahedral Ga (CN: coordination number).

in Table 1 is: $(Si_{3.46}Ga_{0.54})Ga_{2.1}O_{10}(OH)_2,Na_{0.24}$. It is obvious that this structural formula is incorrect, given the Ga excess. However, the existence of a tetrahedral charge is consistent with the Li test and the XANES data. The synthetic Ga-smectite is then a beidellite. Its *d*(06-33) reflection appears at a high value for a dioctahedral smectite (1.51 Å) but is consistent with an octahedral sheet completely filled by Ga^{3+} cations.

Changes in chemical compositions along the series can thus be explained by (i) Al/Ga substitutions in octahedral sites of kaolinite and smectite, (ii) Ga/Si substitutions in tetrahedral sites of smectite, and (iii) various kaolinite to smectite ratios.

This work on Ga/Al substitutions in silicate minerals has shown the potential for Ga^{3+} to be included in the structures of kaolinite and smectite, indicating new potential resources of Ga.

Nevertheless, because of Ga^{3+} - Fe^{3+} similarity, a study on Ga/Fe subtitutions is to be carried out. This should allow for greater understanding of Ga/Al substitutions and hence the best ways of determining economic quantities of Ga.

ACKNOWLEDGMENTS

The staff of LURE are acknowledged for their assistance in XAS measurements and A. Michalowich for his XANES absorption programme. We would also like to thank Ch. Mosser, P. Schroeder, and J. Yvon for their constructive comments.

REFERENCES

Barrios J., Plançon A., Cruz M.I. & Tchoubar C. (1977) Qualitative and quantitative study of stacking in a hydrazine treated kaolinite-relationship with infrared spectra. *Clays Clay Miner*. **25**, 422–429.

Cases J.M., Lietard O., Yvon J. & Delon J.F. (1982) Etudes des propriétés cristallochimiques, morphologiques, superficielles de kaolinites désordonnées. *Bull. Miner*. **105**, 439–455.

Cliff G. & Lorimer G.W. (1975) The quantitative analysis of their specimens. *J. Microsc*. **103**, 203–207.

Delineau T., Allard T., Muller J.P., Barres O., Yvon J. & Cases J.M. (1994) FTIR reflectance vs. EPR studies of structural iron in kaolinites. *Clays Clay Miner*. **42**, 308–320.

Farmer V.C. (1974) The layer silicates. Pp. 331–363 in: *The Infrared Spectra of Minerals.* Mineralogical Society, London.

Greene-Kelly R. (1953) The identification of montmorillonoids in clay. *J. Soil Sci*. **4**, 233–247.

Hiéronymus B., Boulègue J. & Kotschoubey B. (1990) Gallium behaviour in some intertropical environment alterations. *Geosciences of the Earth's Surface and of Mineralogical Formation., 2nd Int. Sym., Aix-en-Provence*, 78–82.

Hoffmann U. & Klemen R. (1950) Verlust des Austauschfähigkeit von Lithiumionen an Bentonit durch Erhitzung. *Z. Anorg. Allg. Chem*. **262**, 95–99.

Jackson, M.L. (1958) *Soil Chemical Analysis*, 3rd ed., Prentice Hall, Englwoods Cliffs, New Jersey.

Katrak F.E. & Agarwal J.C. (1981) Gallium: long-run supply. *J. Metals*, 33–36.

Kato E., Kanaoka S. & Inagaki S. (1977) Infrared spectra of kaolin minerals in OH region (I); on the glass slide method for the measurement of the infrared spectra in OH region of clay minerals. *Rept. Govt. Industr. Agoya*, **26**, 203–210.

De Kimpe C., Kodama H. & Rivard R. (1981) Hydrothermal formation of kaolinite material from aluminosilicate gels. *Clays Clay Miner*. **29**, 446–450.

Lietard O. (1977) *Contribution à l'étude des propriétés physicochimiques, cristallochimiques et morphologiques des kaolins*. PhD thesis, INPL Nancy, France.

Nesbitt H.W. (1977) Estimation of the thermodynamic properties of Na-Ca- and Mg-beidellites. *Can. Miner*. **15**, 22–30.

Petit S. & Decarreau A. (1990) Hydrothermal (200°C) synthesis and crystal chemistry of iron-rich kaolinites. *Clay Miner*. **25**, 181–196.

Petit S., Robert J.L., Decarreau A., Besson G., Grauby O. & Martin F. (1995) Contribution of spectroscopic methods to 2:1 clay characterization. *Bull. Elf Aquitaine Prod*. **19**, 119–147.

Plançon A. & Tchoubar C. (1977) Determination of structural defects in phyllosilicates by X-ray powder diffraction. II. Nature and proportion of defects in natural kaolinites. *Clays Clay Miner*. **25**, 436–450.

Reynolds R.C. Jr. (1985) *NEWMOD a Computer Program for the Calculation of One-Dimensional Diffraction Patterns of Mixed-Layered Clays*. R.C. Reynolds, 8 Brook Rd., Hanover, NH 03744, USA.

Rouxhet P.G., Samudacheata N., Jacobs H. & Anton O. (1977) Attribution of the OH stretching band of kaolinites. *Clay Miner*. **12**, 171–179.

Shannon R.D. (1976) Revised effective ionic radii and systematic studies of interatomic distances in halides and chalcogenides. *Acta Cryst*. **A32**, 751–767.

Siffert B. & Wey R. (1961) Sur la synthèse de la kaolinite à la température ordinaire. *C. R. Acad. Sci*. Paris, **253**, 142–144.

Środoń J., Morgan D.J., Elsinger E.V., Eberl D.D. & Karlinger M. (1986) Chemistry of illite/smectite and end-member illite. *Clays Clay Miner*. **34**, 368–378.

Stubican V. & Roy R. (1961) A new approach of assignment of infra-red absorption bands in layer-structure silicates. *Zeitschrift Kristall.* Bd. **115**, S., 200–214.

Tomura S., Shibasaki Y., Mizuta H. & Kitamura M. (1985) Growth conditions and genesis of spherical and platy kaolinite. *Clays Clay Miner*. **33**, 200–206.

Wolf A. (1967) *Contribution à l'étude du mécanisme de formation des argiles: réaction de la silice en solution avec les cations Al, In, Ni et Cu.* PhD thesis, Univ. Strasbourg, France.